Acoustically-induced bubble growth and phase change dynamics near compliant surfaces

Mauro Rodriguez*, Spencer H. Bryngelson, Tim Colonius

Division of Engineering and Applied Science, California Institute of Technology, Pasadena, CA 91125, USA

Abstract

Biomedical therapies use focused ultrasound to treat pathogenic tissues. The ultrasound waves lead to nucleation, grow and collapse of bubbles. Previous numerical simulations of this process have treated the bubble contents as non-condensible gas, but it is known that phase change affects the bubble dynamics as a function of the driving frequency and waveform. In this study, we incorporate phase change in the six-equation, multiphase model previously implemented in our Multi-component Flow Code (MFC). The implementation is verified with 1D cavitation and shock problems. To highlight the effects of phase change, we simulate the expansion of a 2D bubble near a solid, rigid boundary to observe phase change near the interface.

Keywords: phase change, bubble dynamics, ultrasound, cavitation, material damage

1. Introduction

Bubbles cavitate near compliant surfaces in many hydraulic engineering and biomedical applications. One such example is high-amplitude ultrasound, which is used to treat both soft (e.g., cancer tumors) and hard (e.g., urinary stones) pathogenic tissues. During these therapies, transducers emit focused ultrasound waves which in turn induce cavitation: the tensile portion of the wave initiates and grows initially-small bubbles near the targeted tissue and the compressive part further accelerates their collapse. The resulting shock waves impinge on adjacent surfaces, damaging the target material. It is known that the frequency and driving waveform affects the phase change and bubble contents. We hypothesize that the strength of the shock generated by the bubble and surface impact that loads to the surface can be controlled by the ultrasound amplitude and frequency. Near-surface bubble collapses and phase change have been studied independently, but the relative import of phase change during these bubble oscillations, and how this relates to the impact at the surface, remains unknown.

Experimental investigation of this problem is challenging due to limited optical access and the wide range of spatio-temporal scales associated with the bubble dynamics. Numerical simulations complement these investigations as they are not always limited in this way. For example, the open-source Multi-component Flow Code (MFC) uses a fully Eulerian framework to access these scales [1]. It uses a shock- and interface-capturing method to simulate 3D fluid-structure interaction and multi-scale cavitation problems. Here, it is augmented to investigate the dynamics of a single bubble that grows rapidly due to ultrasound pulses near model pathogenic tissues. Phase change is represented as heat and mass transfer between the components and implemented via a six-equation thermodynamic-disequilibrium model. Coupled evolution equations for the linear elastic contribution to the Cauchy stress tensor account for the model material elasticity.

The model and its implementation are verified via comparison to simulations of underwater multiphase explosion problems. Experimental measurements of the elastic stress in the model

*Corresponding author: mrdz@caltech.edu

materials validate the numerical method. Simulations of acoustically-driven bubble growth with phase change near a rigid wall are investigated.

2. Methods

2.1. Governing Equations

We use the compressible six-equation, multicomponent model for the flow:

$$\frac{\partial \boldsymbol{q}}{\partial t} + \nabla \cdot \boldsymbol{F}(\boldsymbol{q}) + \boldsymbol{h}(\boldsymbol{q}) \nabla \cdot \boldsymbol{u} = \boldsymbol{r}(\boldsymbol{q}), \tag{1}$$

where $\boldsymbol{q}$ is the state vector, $\boldsymbol{F}$ the flux tensor, $\boldsymbol{u}$ the velocity vector, and $\boldsymbol{h}$ and $\boldsymbol{r}$ non-conservative terms involving pressure, thermal, and chemical disequilibrium [7]. Specifically,

$$\begin{aligned}
\boldsymbol{q} &= \left[\ \alpha_1, \ \rho_1\alpha_1, \ \rho_2\alpha_2, \ \rho\boldsymbol{u}, \ \rho_1\alpha_1 e_1, \ \rho_2\alpha_2 e_2 \ \right]^\top, \\
\boldsymbol{F} &= \left[\ \alpha_1, \ \boldsymbol{u}, \ \rho_1\alpha_1\boldsymbol{u}, \ \rho_2\alpha_2\boldsymbol{u}, \ \rho\boldsymbol{u}\otimes\boldsymbol{u} + p\boldsymbol{I}, \ \rho_1\alpha_1 e_1\boldsymbol{u}, \ \rho_2\alpha_2 e_2\boldsymbol{u} \ \right]^\top, \\
\boldsymbol{h} &= \left[\ -\alpha_1, \ 0, \ 0, \ \boldsymbol{0}, \ \alpha_1 p_1, \ \alpha_2 p_2 \ \right]^\top, \\
\boldsymbol{r} &= \left[\ \mu\delta p + Q/\kappa + \dot{m}/\varrho, \dot{m}, -\dot{m}, \boldsymbol{0}, -\mu p_I \delta p + Q + \varepsilon\dot{m}, \mu p_I \delta p - Q - \varepsilon\dot{m} \ \right]^\top,
\end{aligned} \tag{2}$$

where ρ_k, α_k, p_k, and e_k are the phase k density, volume fraction, and specific internal energy, respectively. The velocity vector and identity tensors are denoted $\boldsymbol{u}$ and $\boldsymbol{I}$, respectively. Note that $\sum_k \alpha_k = 1$ and $\sum_k \rho_k\alpha_k = \rho$, where ρ is the mixture density and v is the specific volume. The mixture internal energy (per unit volume) is $\rho e = \sum_k \rho_k\alpha_k e_k$. The total energy per unit volume E comprises the internal and kinetic energies as $E = \rho e + \frac{1}{2}\rho u_k^2$. The total energy is numerical conserved by solving the additional total energy evolution equation [1]. The stiffened gas equation of state relates the pressure, temperature, and density [4]. Considering a single material in two phases (e.g., liquid water and water vapor), the interfacial pressure difference is $\delta p = p_1 - p_2$ and μ is the pressure relaxation parameter. The interfacial relaxation pressure is $p_I = (Z_2 p_1 + Z_1 p_2)/(Z_1 + Z_2)$, where $Z_k = \rho_k a_k^2$ is the phase k acoustic impedance and a_k the phase k speed of sound. Thermal transfer is defined as the temperature difference $Q = \theta(T_2 - T_1)$, where θ is the thermal relaxation parameter. Mass transfer between two phases is defined as the difference between the Gibbs free energies $\dot{m} = \nu(g_2 - g_1)$, where ν is the mass transfer relaxation parameter. Parameters ϱ, κ, and e_I are defined as function of the state variables and detailed in [7]. In principle, the parameters μ, θ, and ν have no physical basis and are assumed to be infinite near the interface and zero elsewhere [6].

2.2. Numerical algorithm

The Multi-component Flow Code (MFC) is used to study phase change in single bubble dynamics [1, 2]. The algorithm uses the third-order accurate total variation diminishing (TVD) Runge–Kutta scheme following the appropriate advective and diffusion numerical constraints. The HLLC approximate Riemann solver is used, with appropriate correction for equations in non-conservative form in conjunction with the high-order accurate primitive variable WENO reconstruction scheme [3]. The first and second derivatives of the diffusion and source terms are computed using an averaged WENO calculation of the velocity gradient.

Two numerical approaches are considered to solve (1): (i) direct computation and (ii) fractional stepping [5]. For (i), the right-hand-side terms of (1) are directly computed with the relations for ϱ, κ, and ε detailed by [7]. The pressure, thermal, and mass relaxation parameters are 10^{10}, 10^8, and 10^{-3}, respectively. These terms are then included in the right-hand-side term of the time

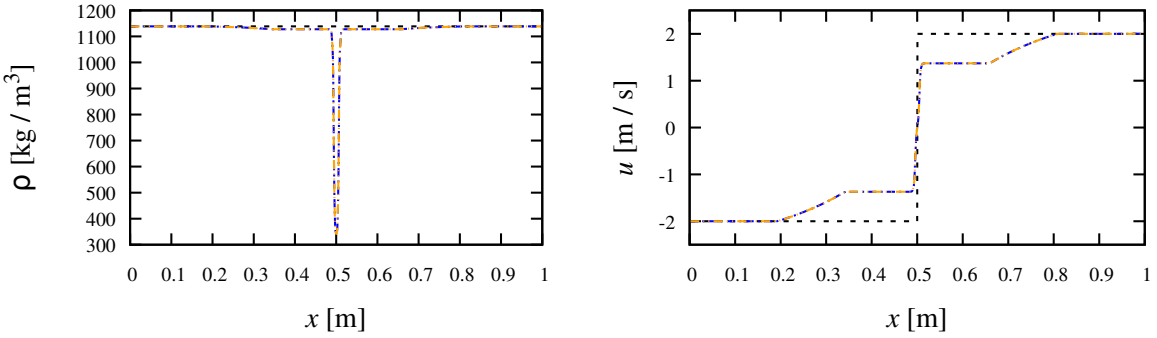

Figure 1: Liquid water-water vapour cavitation problem with $|U| = 2\,\mathrm{m/s}$ at $t = 3.2\,\mathrm{ms}$ for infinite (- - -) and finite (-·-·-) p-pT-pTg relaxation. Dashed black line (- - -) is the initial condition.

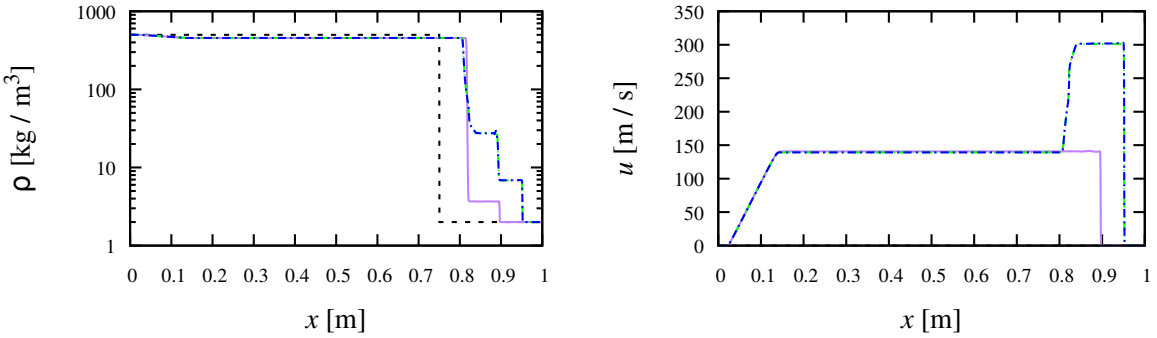

Figure 2: Liquid dodecane-dodecane vapour shock tube problem with pressure ratio 10^3 at $t = 473\,\mu\mathrm{s}$ for p (——), p-pTg (·····), and p-pT-pTg (-·-·-) relaxation. Initial condition: (- - -).

integration. For (ii), within each time step the homogeneous form of (1) is solved first. An infinite relaxation step is then updates the mixture densities and volume fractions to ensure thermodynamic equilibrium [5]. There are three different relaxation procedures: mechanical (p), thermo-mechanical (p–pT), and thermodynamic (p–pT–pTg). The pTg relaxation enables the change of phase. For brevity, we only discuss pTg relaxation herein.

2.3. Verification

To verify the implementation, we consider a liquid water–water vapor cavitation tube problem of [5]. The cavitation tube is initial filled with a mixture of liquid water ($\rho_\ell = 1150\,\mathrm{kg/m^3}$) and water vapor ($\rho_g = 0.63\,\mathrm{kg/m^3}$) at $p = 10^5\,\mathrm{Pa}$. The vapor density was determined such that there is thermal equilibrium, $T_l = T_v = 354.7\,\mathrm{K}$. The vapor volume fraction is set to $\alpha_v = 10^{-2}$. The initial x-direction velocity discontinuity is set at $x = 0.5\,\mathrm{m}$ with $u = -2\,\mathrm{m/s}$ at the left and $u = 2\,\mathrm{m/s}$ at the right. Figure 1 shows the comparison between the finite (direct) and infinite p–pT–pTg relaxation numerical techniques. The density and x-direction velocity match the infinite relaxation results obtained with the second-order accurate methods of [5]. The result shows the p–pT–pTg infinite relaxation approach aptly solving system (1).

We consider the shock tube problem in dodecane liquid and vapor. The problem follows the initial conditions of [6]. There is an initial discontinuity at $x = 0.75\,\mathrm{m}$ with $\rho_\ell = 500\,\mathrm{kg/m^3}$ and $\rho_v = 2\,\mathrm{kg/m^3}$, pressure ratio $p_\ell/p_v = 10^3$, and vapor volume fraction of $\alpha_v = 10^{-8}$. Figure 2 shows the dodecane shock tube problem results for the different phase relaxation approaches at

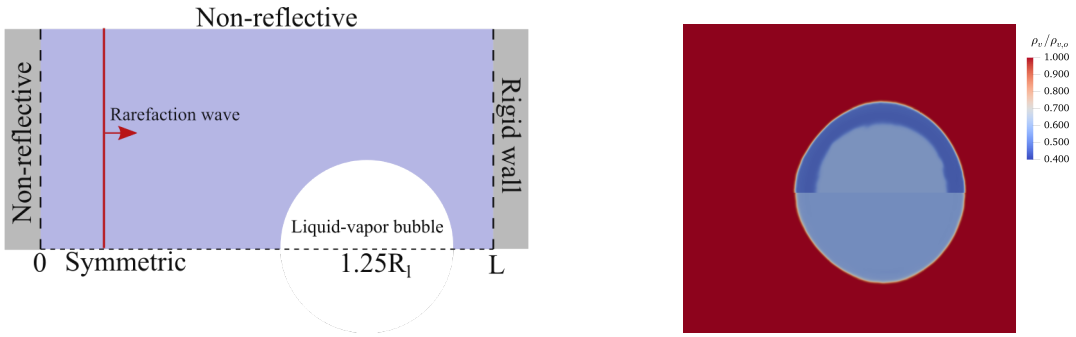

Figure 3: 2D liquid–vapor bubble interacting with a rarefaction wave near a rigid wall. Problem set–up (left) and vapor density contours with p–pT–pTg (top right) and p (bottom right) relaxation.

$t = 473\,\mu s$. The results are similar to those of [6] showing the rarefaction, shock, and contact waves. The additional evaporation wave is observed at $x = 0.8\,m$ for the phase change approaches.

3. Results

We now consider the 2D problem involving a liquid-vapor bubble interacting with a rarefaction wave near a rigid wall. The problem set–up and vapor density contours are shown in figure 3. A right-ward propagating rarefaction wave is used with pressure ratio reduction of $p/p_{\text{atm}} = 10^2$. In absence of the bubble, the rarefaction wave reflects from the right wall and further decreases the pressure by a factor of two. Comparing the vapor density contours enables comparison between the relaxation approaches at the bubble interface. After the rarefaction interacts with the bubble, the bubble expands into the liquid. The reflected wave from the rigid wall furthers the bubble expansion. Thus, the vapor condenses into the liquid phase at the bubble interface. This is observed as a ring of decreased vapor not observed in the p relaxation contour (bottom right).

Acknowledgements

The US Office of Naval Research supported this work under grant number N0014-17-1-2676.

References

[1] S. H. Bryngelson, K. Schmidmayer, V. Coralic, J. C. Meng, K. Maeda, T. Colonius, MFC: An open-source high-order multi-component, multi-phase, and multi-scale compressible flow solver, Comput. Phys. Commun. (2020) 107396.

[2] V. Coralic, T. Colonius, Shock-induced collapse of a bubble inside a deformable vessel, Eur. J. Mech. - B/Fluids 40 (2013) 64–74.

[3] E. Johnsen, T. Colonius, Implementation of WENO schemes in compressible multicomponent flow problems, J. Comput. Phys. 219 (2006) 715–732.

[4] O. Le Métayer, J. Massoni, R. Saurel, Élaboration des lois d'état d'un liquide et de sa vapeur pour les modèles d'écoulements diphasiques, Int. J. Therm. Sci. 43 (2004) 265–276.

[5] M. Pelanti, K. M. Shyue, A mixture-energy-consistent six-equation two-phase numerical model for fluids with interfaces, cavitation and evaporation waves, J. Comput. Phys. 259 (2014) 331–357.

[6] R. Saurel, F. Petitpas, R. Abgrall, Modelling phase transition in metastable liquids: application to cavitating and flashing flows, J. Fluid Mech. 607 (2008) 313–350.

[7] A. Zein, M. Hantke, G. Warnecke, Modeling phase transition for compressible two-phase flows applied to metastable liquids, J. Comput. Phys. 229 (2010) 2964–2998.